Dyes and Pigments 92 (2012) 1361–1369

Contents lists available at SciVerse ScienceDirect

Dyes and Pigments

journal homepage: www.elsevier.com/locate/dyepig

Fluorescent coumarin derivatives with large stokes shift, dual emission and solid state luminescent properties: An experimental and theoretical study

Lijuan Xie [a,b,**], Yinghui Chen [a,b], Wenting Wu [b], Huimin Guo [b], Jianzhang Zhao [b,*], Xuerong Yu [b]

[a] Institute of Molecular Medicine, Huaqiao University, 269 Chenghua North Road, Quanzhou 362021, PR China
[b] State Key Laboratory of Fine Chemicals, School of Chemical Engineering, Dalian University of Technology, E-208 West Campus, 2 Ling-Gong Road, Dalian, Liaoning Province 116024, PR China

ARTICLE INFO

Article history:
Received 14 August 2011
Received in revised form
27 September 2011
Accepted 28 September 2011
Available online 6 October 2011

Keywords:
Coumarin
ESIPT
Fluorescence
Density functional theory
Photochemistry
Photophysics

ABSTRACT

Coumarin derivatives containing 8-benzothiazole (**C-2**) and its difluoroboron bound derivative (**C-3**) were prepared. Both derivatives show dual emission at 322 nm and 513 nm and large Stokes shift (188 nm), compared to the unsubstituted coumarin (**C-1**), which shows emission at 356 nm with small Stokes shift of 46 nm. **C-2** and **C-3** show fluorescence in solid state, in contrast the **C-1** is non-fluorescent in the solid state. The excited state intramolecular proton transfer (ESIPT) process of **C-2** was fully rationalized by DFT/TDDFT calculations with optimization of the ground state (S_0) and excited state (S_1) geometries. TDDFT calculations propose that the large Stokes shift of **C-2** and **C-3** are due to the re-distribution of the frontier molecular orbitals at excited states. Study of the potential energy curve of **C-2** indicated that the dual emission of the **C-2** is due to the simultaneous S_1 and S_3 emission, not the rotamer of the enol form.

1. Introduction

Coumarin derivatives have been widely used in fluorescent molecular probes, electroluminescence, light-harvesting molecular assemblies or photovoltaics [1–7]. However, the unsubstituted coumarin (7-hydroxyl-4-methyl-coumarin) fluorophore suffers from disadvantages of small Stokes shift, which is detrimental to the applications of coumarin, such as for fluorescent molecular probes, etc [1,4]. Therefore, it is of great interest to prepare coumarin derivatives that show large Stokes shifts. Concerning this aspect, one approach is to extend the π-conjugation framework of the fluorophore [5,8–10]. However, with red-shifted emission wavelength, the fluorescence quantum yield usually decreases, due to the energy gap law [11]. Thus a strategy has to be employed to extend the emission to the red-end of the spectra, but at the same time, to maintain high fluorescence quantum yields.

In order to address the aforementioned challenges, herein we prepared benzothiazole-containing coumarin derivatives (**C-2**, **C-3** was prepared by complexation with BF_3. Scheme 1) to employ the excited state intramolecular proton transfer (ESIPT) to produce large Stokes shift [12,13]. We found that the emission wavelength was extended from 356 nm for the parent compound (**C-1**) to the 513 nm for the new compounds (**C-2** and **C-3**). The Stokes shift of the derivatives is up to 188 nm, compared to the small Stokes shift of 46 nm for the parent compound **C-1**. Furthermore, the fluorescence quantum yields of the derivatives are higher than the parent compound (**C-1**). Significant dual emission (at 363 nm and 513 nm) was observed for **C-2**. Based on density functional theory (DFT) calculations for ground state and excited state, the ESIPT process was fully rationalized. We exclude the previously proposed possibility of the rotamer to be responsible for the dual emission [14]. Instead, we propose that the dual emission is due to the radiative decay of the S_1 and S_3 excited states of **C-2**. This assumption is supported by the dual emission of **C-3**, for which the enol structure does not exist. Our complementary experimental and theoretical investigation of the coumarin fluorophores will be useful for design of new coumarin based fluorophores that show red-shifted emission, large Stoke shift and solid state luminescence property.

2. Experimental section

2.1. General information

NMR spectra were measured on a 400 MHz Varian Unity Inova spectrophotometer. Mass spectra were recorded with a Q-TOF

* Corresponding author. Tel./fax: +86 411 8498 6236.
** Corresponding author. Institute of Molecular Medicine, Huaqiao University, 269 Chenghua North Road, Quanzhou 362021, PR China.
E-mail addresses: xielijuan@hqu.edu.cn (L. Xie), zhaojzh@dlut.edu.cn (J. Zhao).

0143-7208/$ – see front matter © 2011 Elsevier Ltd. All rights reserved.
doi:10.1016/j.dyepig.2011.09.023

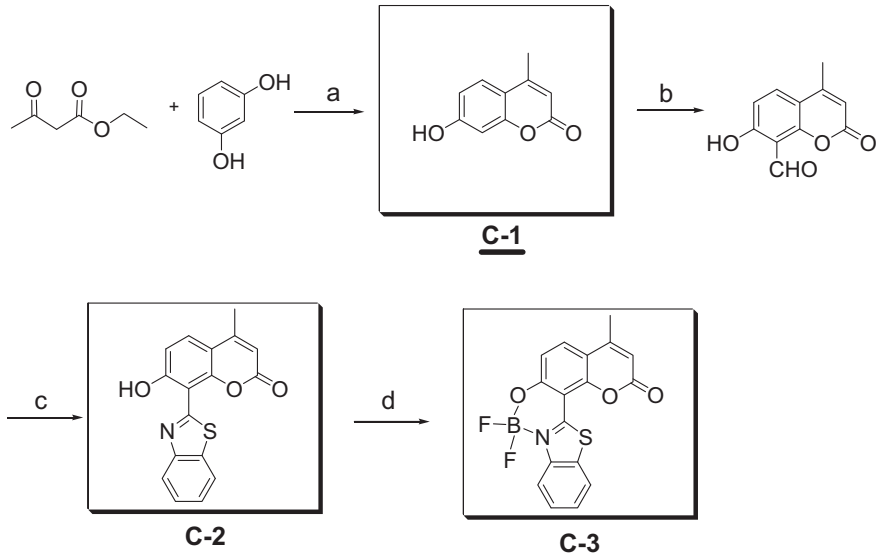

Scheme 1. Synthesis of the compounds **C-1**, **C-2** and **C-3**. (a) THF, 96% H_2SO_4, reflux for 3 h. (b) Hexamine, glacial acetic acid, 95 °C, 5.5 h; 20% HCl, 70 °C, 1 h. (c) ethyl cyanoacetate, benzoic acid, *n*-butanol, reflux for 5 h. (d) BF_3• OEt_2, TEA, CH_2Cl_2.

Micro MS spectrometer. UV–Vis spectra were carried on an Agilent HP8453 UV–visible spectrophotometer. Fluorescence spectra were recorded on a JASCO FP-6500 and Shimadzu 5301PC spectrofluorometer. Luminescence quantum yields were measured with quinine sulfate as the standard ($\Phi_F = 54.6\%$ in 0.05 M H_2SO_4). Luminescence lifetimes were measured on an OB920 fluorescence lifetime spectrometer (Edinburgh Instruments, U.K.).

2.2. Synthesis

2.2.1. ***C-1*** *[15]*

Concentrated sulphuric acid (2 mL) was added into the solution of resorcinol (11.0 g, 0.1 mol) in tetrahydrofuran (THF, 40 mL), then acetoacetic ester (13.0 g) was added dropwise. The reaction mixture was refluxed for 3 h and monitored by TLC until the resorcinol was completely consumed. After cooling, the solution was poured into ice water (100 mL), yellow precipitate was collected by filtration and washed with cold water. Pale yellow solid was obtained by recrystallization with 95% ethanol (11.3 g, Yield: 64 %). M.p. 185.0 °C–186.0 °C. ^{1}H NMR (400 MHz, CD_3OD), δ 7.61 (d, 1H, $J = 8.9$ Hz), 6.83 (d, 1H, $J = 10$ Hz), 6.70 (s, 1H), 6.10 (s, 1H), 2.42 (s, 3H). TOF MS EI$^+$ calcd 176.0473, found 176.0469.

2.2.2. *8-Formyl-7-hydroxy-4-methyl-coumarin*

7-Hydroxy-4-methyl-coumarin (5.3 g, 0.03 mol) and hexamine (9.8 g, 0.07 mol) in glacial acetic acid (50 mL) were refluxed for 5.5 h, and then 20% HCl (75 mL) was added and the solution was heated for 1 h. After cooling, the reaction mixture was extracted with ether, and the combined organic layers were evaporated under reduced pressure. The residue was poured into ice water, and pale yellow solid of 8-formyl-7-hydroxy-4-methyl-coumarin was obtained. The further purification was carried out by recrystallization with hot ethanol to obtain a light yellow powder (612.1 mg, Yield 10%). M.p. 180 °C–181.0 °C (lit. 120.0 °C–122.0 °C) [15]. ^{1}H NMR (400 MHz, $CDCl_3$), δ 12.23 (s, 1H); 10.63 (s, 1H); 7.52 (d, 1H, $J = 9$ Hz); 6.92 (d, 1H, $J = 9$ Hz); 6.21 (s, 1H); 2.43 (s, 3H).

2.2.3. ***C-2***

A mixture of 8-formyl-7-hydroxy-4-methyl-coumarin (204.0 mg, 1 mmol), ethyl cyanoacetate (0.11 mL, 1 mmol) and *o*-aminothiophenol (0.11 mL, 1 mmol) in *n*-butanol (10 mL) containing benzoic acid (0.3 mmol) was refluxed for 5 h. After cooling, the solid was filtered and washed with water. Further purification was employed

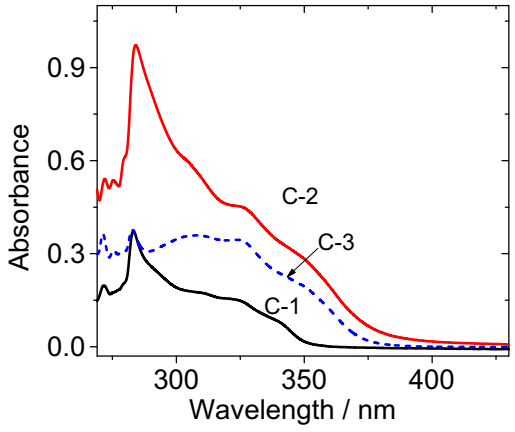

Fig. 1. UV–Vis absorption of **C-1**, **C-2** and **C-3** (1.0×10^{-5} mol/L) in toluene at room temperature 20 °C.

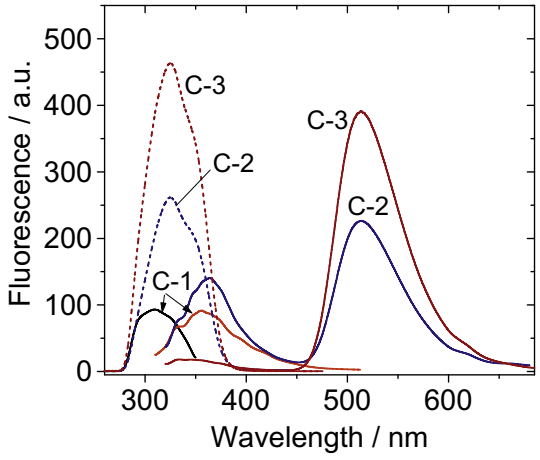

Fig. 2. Excitation spectra and emission spectra of **C-1**, **C-2** and **C-3** (1.0×10^{-5} mol/L) in toluene at room temperature. $\lambda_{ex/C-1} = 300$ nm, $\lambda_{ex/C-2} = 310$ nm, $\lambda_{ex/C-3} = 310$ nm 20 °C.

Table 1
Photophysical properties of **C-1**, **C-2** and **C-3**.

Compounds	λ_{abs} (/nm)[a]	λ_{em} (/nm)[a]	ε (M^{-1} cm^{-1})[a]	Φ_F[a]	τ_F(ns)[a]
C-1	325	356	15,000	2.56%	11.84
C-2	322	363, 514	46,000	4.07%	8.73 (360 nm), 2.44 (530 nm)
C-3	322	340, 514	34,000	7.69%	9.97 (360 nm), 2.59 (530 nm)

[a] Measurements were performed in toluene solvent. Fluorescence quantum yields were measured with quinine sulfate ($\Phi_F = 54.6\%$ in 0.05 M H_2SO_4) as the reference.

with column chromatography (silica gel, dichloromethane), affording **C-2** as a pale yellow solid (170.0 mg, Yield 55%) [10]. M.p. 240.0 °C–240.8 °C. ^{1}H NMR (400 MHz, $CDCl_3$), δ 8.07 (d, 1H, $J = 8.1$ Hz); 8.02 (d, 1H, $J = 7.9$ Hz); 7.64 (d, 1H, $J = 8.8$ Hz); 7.59 (m, 1H, $J = 8.3$ Hz, 7.0 Hz); 7.50 (m, 1H, $J = 7.3$ Hz, 8.7 Hz); 7.11 (d, 1H, $J = 8.9$ Hz); 6.22 (s, 1H); 2.47 (s, 3H). TOF MS EI$^+$ calcd 309.0461, found 309.0460.

2.2.4. *C-3*

8-benzothiazoly-7-hydroxy-4-methyl-coumarin (61.8 mg, 0.2 mmol) was resolved in CH_2Cl_2 (10 mL), and then one drop of triethylamine and $BF_3.OEt_2$ (0.1 mL) were added successively. The reaction solution was stirred for 30 min. Then crude product was purified by silica gel column chromatography (eluted with CH_2Cl_2) to give **C-3** as a pale yellow solid (17.9 mg, Yield 25%). M.p. 233.7 °C–234.1 °C. ^{1}H NMR (400 MHz, $CDCl_3$), δ 8.07 (d, 1H, $J = 9.1$ Hz); 8.02 (d, 1H, $J = 7.9$ Hz); 7.64 (d, 1H, $J = 8.7$ Hz); 7.59 (m, 1H, $J = 6.7$ Hz, 8.2 Hz); 7.50 (m, 1H, $J = 7.9$ Hz, 7.6 Hz); 7.11 (d, 1H, $J = 8.9$ Hz); 6.22 (s, 1H); 2.48 (s, 3H). TOF MS EI$^+$ calcd 309.0461, found 309.0460.

2.3. Computational methodology

All the calculations were based on density functional theory (DFT) with B3LYP functional and 6-31G(d) basis set. Toluene was used as solvent in all the calculations (PCM model). The UV–vis absorption of the compounds (vertical excitation) was calculated with the TDDFT methods based on the optimized ground state geometry (S_0 state). For the fluorescence emission, the emission wavelength was calculated based on the optimized excited states geometries (S_1, S_2 or S_3 state). All these calculations were performed with Gaussian 09W [16].

3. Results and discussion

3.1. UV–vis absorption and fluorescence emission spectra

The UV–vis absorptions of the compounds were presented in Fig. 1. It was observed that the absorption of **C-2** and **C-3** were enhanced compared to that of **C-1**. Furthermore, the absorption of **C-2** and **C-3** are relatively red-shifted compared to the absorption of **C-1** [9]. The molar extinction coefficients of **C-1** at 325 nm is 15,000 M^{-1} cm^{-1}. **C-2** and **C-3** show ε value of 45,000 and 34,000 M^{-1} cm^{-1} at the same wavelength.

The fluorescence excitation and emission spectra of the compounds were studied (Fig. 2). The parent compound **C-1** shows excitation band at 310 nm and emission band at 356 nm. Thus the Stokes shift is 46 nm. For **C-2**, however, the excitation maximum is at 325 nm and the emission band is significantly red-shifted to 513 nm. Thus the Stokes shift of **C-2** is 188 nm. **C-3** shows excitation and emission bands similar to that of **C-2**. To the best of knowledge, the Stokes shifts of **C-2** and **C-3** are larger than most of the coumarin fluorophores [1,4,9]. Since the spectra were measured under the same conditions thus we can anticipate high fluorescence quantum yields for **C-2** and **C-3** compared to **C-1**.

Interestingly, dual emission bands at 363 nm and 514 nm were observed for **C-2**. Similarly minor emission band at 340 nm was observed for **C-3**, along the major emission band at 514 nm. To the best of knowledge, very few coumarin fluorophores show the dual emission properties. The multi emission of organic fluorophores is in particular interesting for applications such as white light electroluminescence or luminescent bioimaging [9,17–19].

The photophysical properties of the compounds were summarized in Table 1. Interestingly, **C-2** shows unexpected high fluorescence quantum yields ($\Phi_F = 4.07$ %) than most of the fluorophores that show excited state intramolecular proton transfer (ESIPT), which usually give quantum yield of less than 1% [12].

The solvent polarity dependence of the compounds' emission is studied (Fig. 3). For **C-1**, the emission is greatly red-shifted in highly polar solvents such as methanol and water. For **C-2**, the emission intensity is decreased by increasing the solvent polarity. We noticed that the dual emission of **C-2** is persistent in most solvents. Interestingly, we found that the intensity varied with the solvent polarity, but the emission wavelength did not change. This property is different from the normal behavior of organic fluorophores that gives red-shifted emission in polar solvents [20]. We tentatively assign the decreased emission intensity of **C-2** in polar solvents to a non-radiative decay channel which is enhanced by high polarity. Considering the potential ESIPT, the dual emission can be

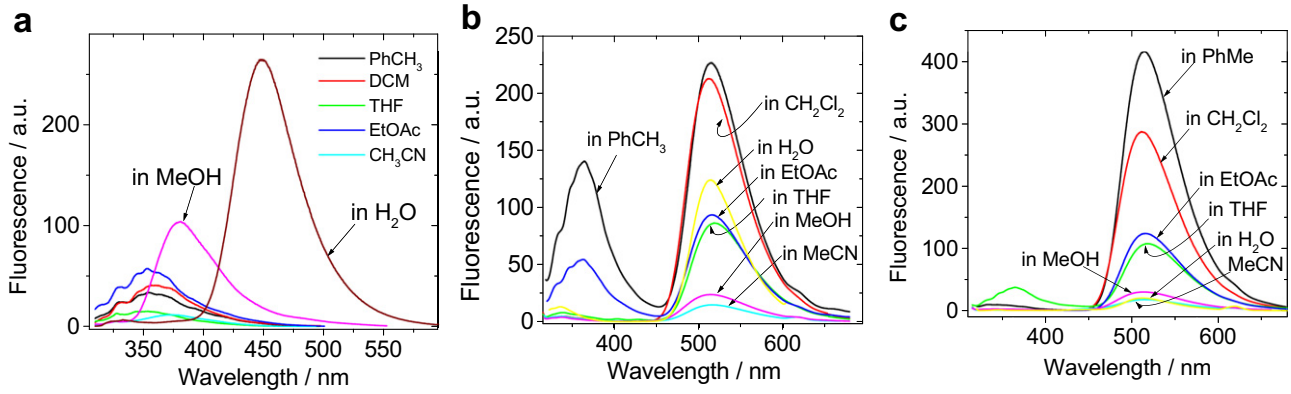

Fig. 3. Emission spectra of (a) **C-1** and (b) **C-2** (1.0×10^{-5} mol/L) in different kinds of solvent at room temperature. $\lambda_{ex/C\text{-}1} = 300$ nm. $\lambda_{ex/C\text{-}2} = 310$ nm. (c) Emission spectra of **C-3** (1.0×10^{-5} mol/L) in different kinds of solvent at room temperature. $\lambda_{ex/C\text{-}3} = 310$ nm, 20 °C.

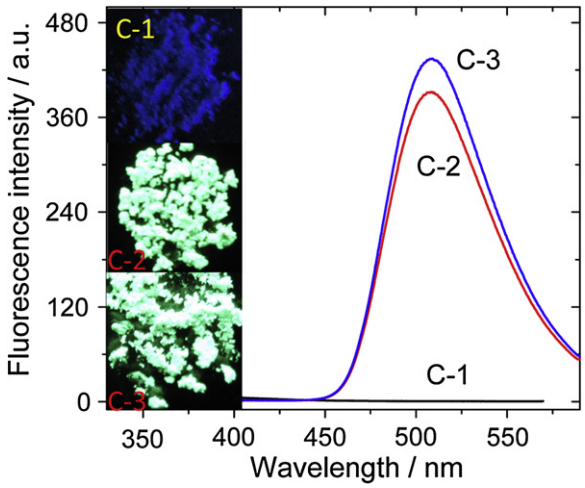

Fig. 4. Emission spectra of solid **C-1**, **C-2** and **C-3** at room temperature. $\lambda_{ex/C\text{-}1} = 300$ nm, $\lambda_{ex/C\text{-}2} = 310$ nm, $\lambda_{ex/C\text{-}3} = 310$ nm 20 °C.

tentatively assigned to the enol rotamer and the cis keto form (produced by the ESIPT) [14].

We found that **C-2** and **C-3** are highly fluorescent in solid state (Fig. 4). Intense greenish or blue emission were observed upon illumination of the solid with the handhold UV lamp (365 nm). By comparison **C-1** is non-fluorescent in the solid state. Materials fluorescent in solid state could be used for electroluminescence devices [21].

Table 2
Electronic excitation energies (eV) and corresponding oscillator strengths (*f*), main configurations and CI coefficients of the low-lying electronically excited states of **C-2** calculated by TDDFT//B3LYP/6-31G(d), based on the DFT//B3LYP/6-31G(d) optimized ground state and excited state geometries.

	Electronic transition[a]	TDDFT//B3LYP/6-31G(d)			
		Energy	*f*[b]	Composition[c]	CI[d]
Excitation	$S_0 \rightarrow S_1$	3.65 eV/ 340 nm	0.2620	HOMO → LUMO	0.5982
				HOMO − 1 → LUMO	0.1717
				HOMO → LUMO + 1	0.3191
	$S_0 \rightarrow S_2$	3.80 eV/ 326 nm	0.2571	HOMO − 1 → LUMO	0.5910
				HOMO → LUMO	0.2943
				HOMO → LUMO + 1	0.2230
Emission	$S_0 \rightarrow S_1$[e]	2.51 eV/ 495 nm	0.2138	HOMO → LUMO	0.7024
	$S_0 \rightarrow S_2$	3.42 eV/ 363 nm	0.0000	HOMO − 2 → LUMO	0.6938
				HOMO − 2 → LUMO + 1	0.1041
	$S_0 \rightarrow S_3$[f]	3.44 eV/ 361 nm	0.3541	HOMO → LUMO + 1	0.6713

[a] Only selected excited states were considered. The numbers in parentheses are the excitation energy in wavelength.
[b] Oscillator strength.
[c] Only the main configurations are presented.
[d] Coefficient of the wavefunction for each excitations. The CI coefficients are in absolute values.
[e] Based on the optimized S_1 state geometry.
[f] Based on the optimized S_3 state geometry.

3.2. DFT calculations: rationalize the excitation and emission spectra

Recently theoretical calculations are becoming attractive for study of the fluorescence or molecular probes [22,23]. Previously

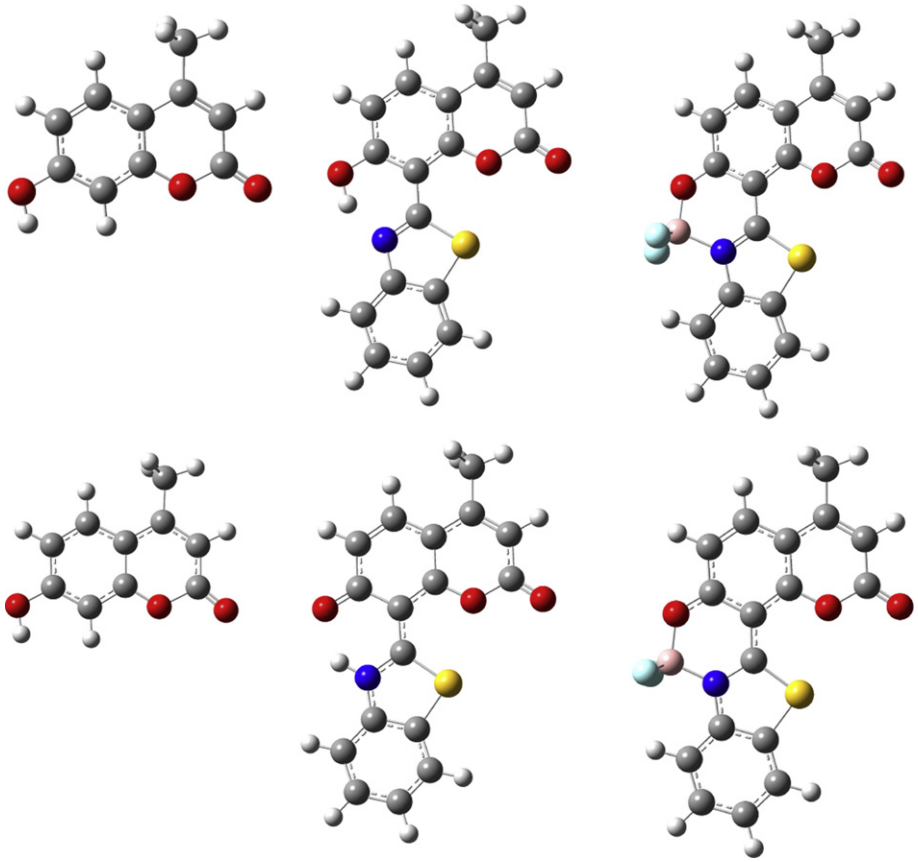

Fig. 5. Optimized ground state (S_0 state, top row) and the singlet excited state (S_1 state, bottom row) geometry of the compounds **C-1**, **C-2** and **C-3**. Solvent toluene was considered in the calculation (PCM model). Calculated at B3LYP/6-31g(d) level with Gaussian 09W.

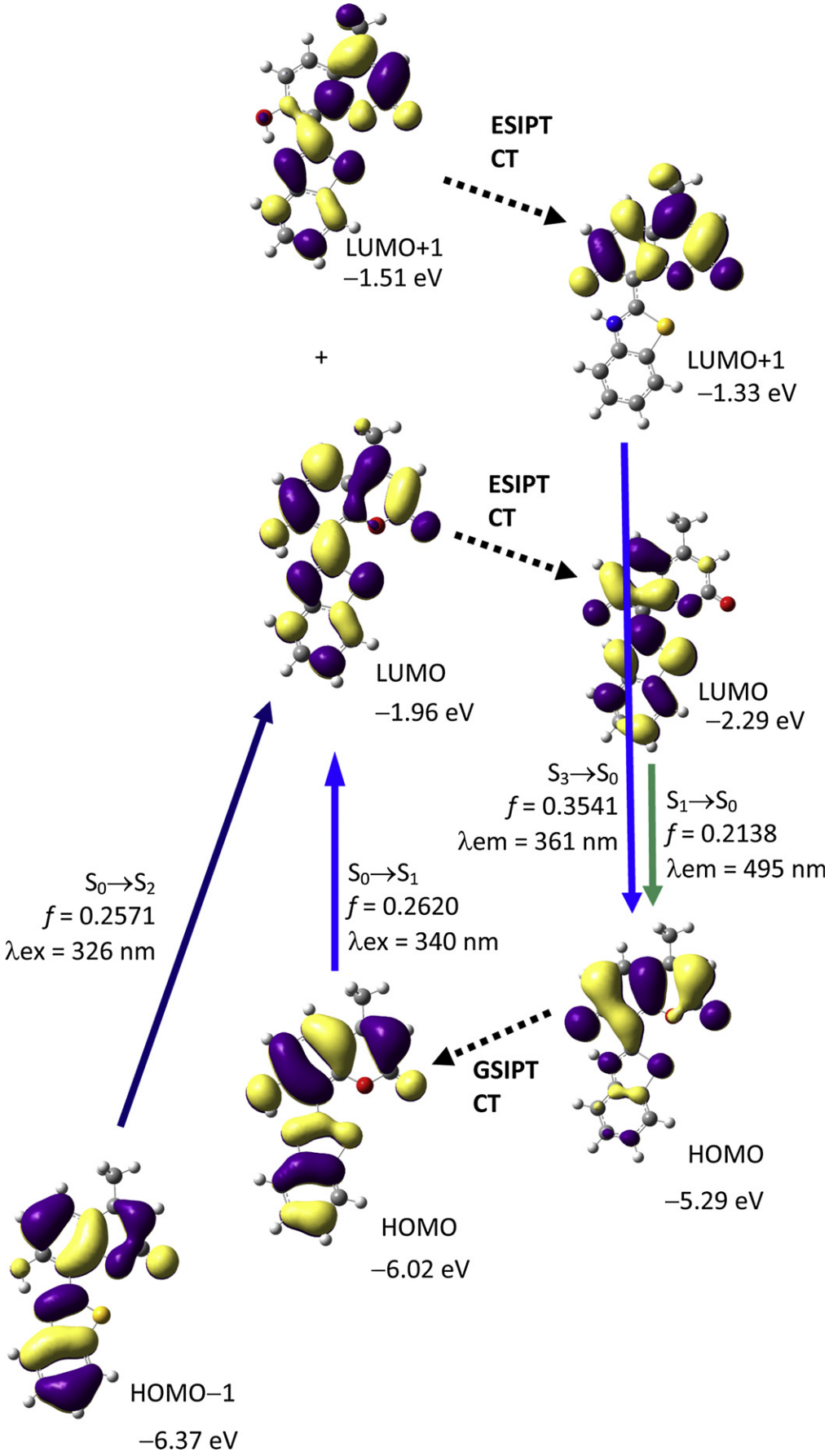

Fig. 6. Frontier MOs involved in the excitation and emission of **C-2** and rationalization of the dual emission of **C-2** and the ESIPT process. The vertical excitation (UV−vis absorption) is calculated based on the optimized ground state geometry (S_0) and the emission is calculated based on the optimized excited state geometry. Calculated at DFT//B3LYP/6-31G(d) level with Gaussian 09W. ESIPT stands for excited-state-intramolecular-proton-transfer; CT stands for conformation transformation; GSIPT stands for ground state intramolecular proton transfer.

with DFT calculations we studied the fluorescence sensing mechanism of thiol probes [24–27], the emission of phosphorescent transition metal complex, etc [28]. The UV–vis absorption and the fluorescence emission (include the dual emission) of the compounds described herein were investigated by theoretical calculations based on the density functional theory (DFT) method.

Firstly geometry of the compounds at ground state (S_0) and the singlet excited state (S_1) were optimized (Fig. 5). Generally the compounds take coplanar geometry at the S_0 state. For **C-2**, we found that the optimized ground state (S_0) is the enol form. This is in line with the reported result of the 2-(2′-hydroxynaphthyl) benzazoles compounds [29]. The lowest-lying excited state (S_1) of the compounds were also optimized. Interestingly, we found that that **C-2** changed to the keto form at the S_1 excited state, as a result of the ESIPT (please note the initial structure for the optimization is enol form). This theoretical prediction is in full agreement with the previous experimental results of the similar compounds [29,30].

In order to study the UV–vis absorption and the fluorescence emission of the compounds, the time-dependent DFT (TDDFT) calculations were carried out (Table 2). The calculated UV-vis absorption is in good agreement with the experimental results (Table 1). For example, the calculated absorption maxima is at 340 nm, which is very close to the experimentally observed absorption at 325 nm (Fig. 1). The frontier molecular orbitals (MOs) are distributed on the whole π-conjugation framework (Fig. 6).

In order to study the emission of **C-2**, the $S_0 \rightarrow S_1$ excitation energy was calculated with the TDDFT method based on the optimized S_1 state geometry. The calculated S_0–S_1 energy gap, i.e. the emission wavelength, is 495 nm (Table 2), which is in good agreement with the experimental results (513 nm, Fig. 2). The frontier MOs involved in the emission of **C-2** were presented in Fig. 6. Compared to the MOs of the ground state (S_0 state), the MOs at S_1 state is more localized. For example, the HOMO is localized in the coumarin core and the LUMO is more localized on the benzothiazole moiety, which are different from the case of MOs at the S_0 state. Furthermore, we found that the LUMO of **C-2** at the S_1 state is more stabilized by 0.33 eV than the LUMO at the S_0 geometry. However, the HOMO at the S_1 state is destabilized by 0.73 eV (based on optimized S_1 state geometry). The much smaller HOMO-LUMO energy gap at the S_1 geometry than that at the S_0 geometry can be used to rationalize the large Stokes shift of **C-2**. We attribute the different HOMO–LUMO energy gap to the ESIPT process, which is clearly predicted by the DFT/TDDFT calculations.

For **C-1**, however, no such large geometry changes were observed for S_1 and S_0 state, and a small Stokes shift was observed for **C-1**. This theoretical approach to predict the emission property of organic fluorophores can be used for design of new fluorophore with large Stokes shift.

We found a higher excited state S_3 with emission wavelength of 361 nm, this is consistent with the emission band of **C-2** at 363 nm.

Table 3
Electronic excitation energies (eV) and corresponding oscillator strengths (*f*), main configurations and CI coefficients of the low-lying electronically excited states of enol *rotamer* **C-2** calculated by TDDFT//B3LYP/6-31G(d), based on the DFT//B3LYP/6-31G(d) optimized ground state geometries.

	Electronic transition	TDDFT//B3LYP/6-31G(d)			
		Energy[a]	*f*[b]	Composition[c]	CI[d]
Excitation	$S_0 \rightarrow S_1$	3.97 eV/ 312 nm	0.1648	HOMO → LUMO	0.5958
				HOMO − 1 → LUMO	0.1805
				HOMO → LUMO + 1	0.2961
	$S_0 \rightarrow S_2$	4.18 eV/ 297 nm	0.2589	HOMO → LUMO	0.3238
				HOMO → LUMO + 1	0.6118
Emission	$S_0 \rightarrow S_1$	3.35 eV/ 370 nm	0.1267	HOMO → LUMO	0.6559
				HOMO → LUMO + 1	0.2065
				HOMO − 1 → LUMO	0.1311
	$S_0 \rightarrow S_2$	3.71 eV/ 334 nm	0.6068	HOMO − 1 → LUMO	0.6800
				HOMO → LUMO	0.1365

[a] Only selected excited states were considered. The numbers in parentheses are the excitation energy in wavelength.
[b] Oscillator strength.
[c] Only the main configurations are presented.
[d] Coefficient of the wavefunction for each excitations. The CI coefficients are in absolute values.

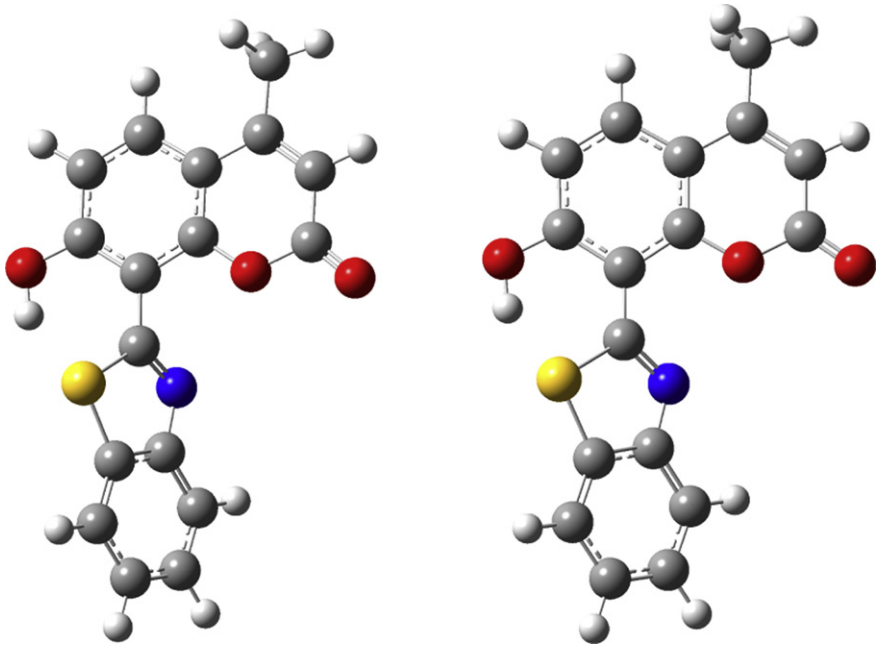

Fig. 7. Geometry of the **C-2** *enol* rotamer at the ground state (S_0, left) and the singlet excited state (S_1, right). Solvent toluene was considered in the calculation (CPCM model). Calculated at B3LYP/6-31g(d) level with Gaussian 09W. The dihedral angle: S_0 state, dihedral angle: 60°; S_1 state, dihedral angle: 33.9°.

Considering the large energy gap between the S_3 and S_1 state, we propose that emissive transition of $S_3 \rightarrow S_0$ is possible [31]. This postulation is supported by the emission of **C-3**, for which there is no ESIPT (e.g. no enol rotamer exist), but the compound still show dual emission. This postulation is against the previous claim that the minor emission at shorter wavelength is due to the enol rotamer at the ground state [29,30].

3.3. *Is rotamer responsible for the emission at shorter wavelength of the dual emissive **C-2**?*

In order to study the property of the anticipated enol rotamer of **C-2**, the proposed enol rotamer structure at the S_0 and S_1 state were optimized (Fig. 7). For the ground state geometry, the coumarin core and the benzothiazole of the molecule take a twisted

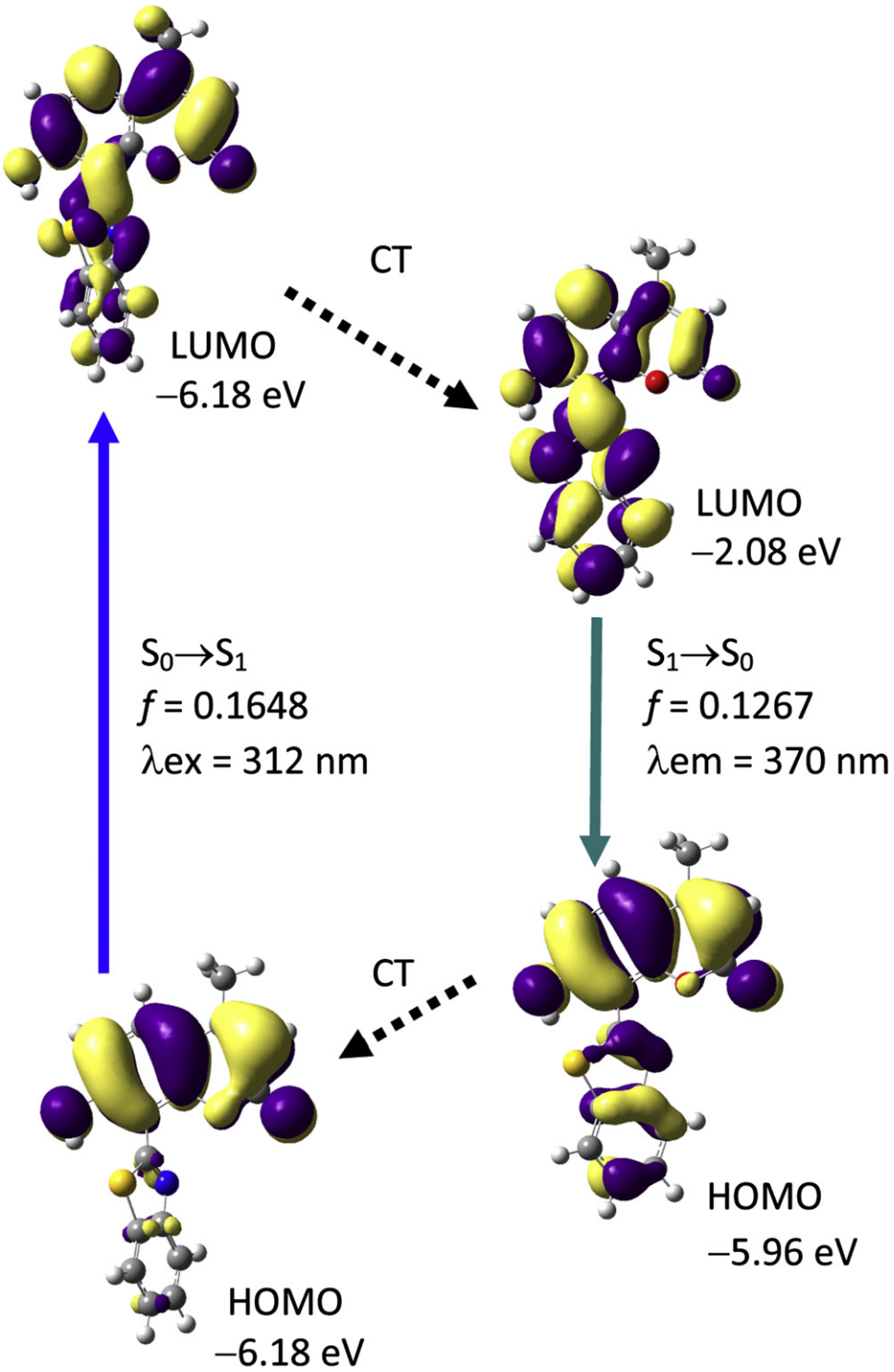

Fig. 8. The frontier MOs involved in the vertical excitation and the emission of **C-2** enol rotamer. Calculated with TDDFT based on the optimized ground state (S_0) and the lowest-lying singlet excited state (S_1) geometry. Solvent toluene was considered in the calculation. Calculated at B3LYP/6-31g(d) level with Gaussian 09W. CT stands for conformation transformation.

conformation, with dihedral angle of 60°. At the S_1 state, however, the two components takes a more coplanary geometry, the dihedral angle is 33.9°.

The UV–vis absorption and the emission of enol rotamer were calculated based on the optimized S_0 state and S_1 state geometry, respectively, with the TDDFT method (Table 3). The calculated absorption band is located at 312 nm, which is much shorter than the normal enol form (Table 2). The HOMO and LUMO involved in the vertical excitation were presented in Fig. 8. HOMO is localized in the coumarin core and the LUMO is localized in the coumarin and the benzothiazole moeity and basically $S_0 \rightarrow S_1$ is a charge transfer excitation. The emission of the enol form is calculated as 370 nm, which is in good agreement with the experimentally observed emission band of **C-2** at 363 nm.

In order to study the possibility of the co-existence of the rotamer (Fig. 7) and the enol form (Fig. 5), we studied the potential energy curve of the **C-2** with variation of the dihedral angle of the C–C bond which connects the coumarin core and the benzothiazole moiety (Fig. 9). Although the rotamer as a local minimum was obtained with DFT geometry optimization (Fig. 7), the potential energy curve gives a very small energy barrier of 0.8 kJ mol^{-1} for the transformation of rotamer to the intramolecular hydrogen bonded enol form (Fig. 5). Thus it is impossible for the rotamer (Fig. 8) to exist at room temperature. Therefore, we propose that the dual fluorescence of **C-2** is due to the $S_1 \rightarrow S_0$ and $S_3 \rightarrow S_0$ emission of the enol form of **C-2**, not the emission from the enol form and the rotamer. The dual emission of **C-2** is fully rationalized by the TDDFT calculations (Table 2).

4. Conclusions

Coumarin derivatives with 8-benzothiazole (**C-2**) and its difluoroboron bound derivative (**C-3**) were prepared. Both derivatives show dual emission at 363 nm and 513 nm and large Stokes shift (188 nm), compared to the parent coumarin (**C-1**) with emission at 356 nm and a small Stokes shift of 46 nm. **C-2** and **C-3** show fluorescence at solid state. The ESIPT process of **C-2** was fully rationalized by DFT/TDDFT calculations, which suggest an enol form for the ground state (S_0) but keto form at the excited state (S_1). The large Stokes shift of the emission of **C-2** and **C-3** are attributed to the re-distribution of the frontier molecular orbitals by TDDFT calculations (optimization of the singlet excited states). The potential energy curve of the **C-2** with variation of the dihedral angle between the coumarin core and the benzenthioazole moiety indicated a very small barrier for the transformation of the rotamer to the enol form (0.8 kJ mol^{-1}), thus the previously proposed rotamer form is impossible to co-exist with the enol form of **C-2**. Therefore we propose the dual emission of the **C-2** is due to the simultaneous S_1 and S_3 emission, which are fully rationalized by TDDFT calculations (with optimization of the excited states). Our findings will be useful for design of new fluorescent dyes with large Stokes shift and to study the photophysical properties of ESIPT fluorescent dyes, such as those with 2-(2′-hydroxyphenyl)-benzothiazole structures.

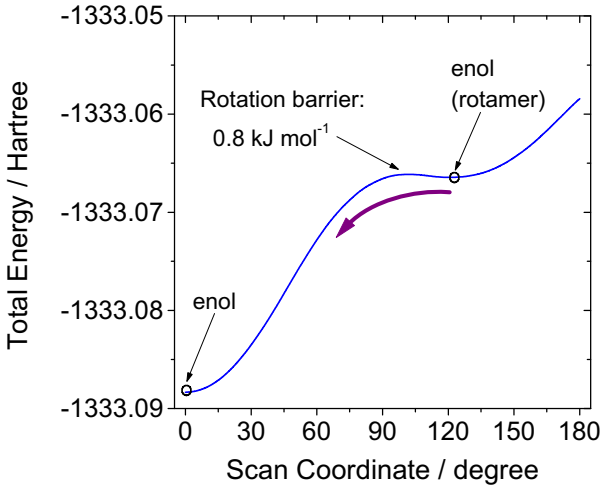

Fig. 9. Potential energy curve of **C-2** with variation of the dihedral angle of C–C bond at the ground state. Calculated at the 6-31g(d)/B3LYP level with Gaussian 09W.

Acknowledgments

We thank the National Natural Science Foundation of China (NSFC) (20972024 and 21073028), Fundamental Research Funds for the Central Universities (DUT10ZD212 and DUT11LK19), The Royal Society (UK) and NSFC (China) for the China–UK Cost-Share Program (21011130154), the State Key Laboratory of Fine Chemicals (KF0802) and the Ministry of Education of China (SRFDP-200801410004 and NCET-08-0077) for financial support.

Appendix. Supplementary data

Supplementary data associated with this article can be found in the online version, at doi:10.1016/j.dyepig.2011.09.023.

References

[1] Lin WY, Long LL, Tan W. A highly sensitive fluorescent probe for detection of benzenethiols in environmental samples and living cells. Chem Commun 2010;46:1503–5.
[2] Park S, Kwon JE, Kim SH, Seo J, Chung K, Park SY, et al. A white-light-emitting molecule: frustrated energy transfer between constituent emitting centers. J Am Chem Soc 2009;131:14043–9.
[3] Lin WY, Long LL, Feng JB, Wang B, Guo CC. Synthesis of meso-coumarin-conjugated porphyrins and investigation of their luminescence properties. Eur J Org Chem; 2007:4301–4.
[4] Li HQ, Cai L, Li JX, Hu YX, Zhou PP, Zhang JM. Novel coumarin fluorescent dyes: synthesis, structural characterization and recognition behavior towards Cu (II) and Ni (II). Dyes Pigments 2011;91:309–16.
[5] Seo KD, Song HM, Lee MJ, Pastore M, Anselmi C, De AF, et al. Coumarin dyes containing low-band-gap chromophores for dye-sensitised solar cells. Dyes Pigments 2011;90:304–10.
[6] Xu ZW, Ding GH, Zhong GY, Xing GC, Li FY, Huang W, et al. Color tunable organic light-emitting diodes using coumarin dopants. Res Chem Intermed 2008;34:249–56.
[7] Lim NC, Schuster JV, Porto MC, Tanudra MA, Yao LL, Freake HC, et al. Coumarin-based chemosensors for zinc (II): toward the determination of the design algorithm for CHEF-type and ratiometric probes. Inorg Chem 2005;44:2018–30.
[8] Schiedel MS, Briehn CA, Bäuerle P. Single-compound libraries of organic materials: parallel synthesis and screening of fluorescent dyes. Angew Chem Int Ed 2001;40:4677–80.
[9] Jagtap AR, Satam VS, Rajule RN, Kanetkar VR. The synthesis and characterization of novel coumarin dyes derived from 1,4-diethyl-1,2,3,4-tetrahydro-7-hydroxyquinoxalin-6-carboxaldehyde. Dyes Pigments 2009;82:84–9.
[10] Zhou SH, Jia JH, Gao JR, Han L, Li YJ, Sheng WJ. The one-pot synthesis and fluorimetric study of 3-(2′-benzothiazolyl) coumarins. Dyes Pigments 2010;86:123–8.
[11] Lakowicz JR. Principles of fluorescence spectroscopy. 2nd ed. New York: Kluwer Academic/Plenum Publishers; 1999. p. 75.
[12] Kwak MJ, Kim YM. Photostable BF_2-chelated fluorophores based on 2-(2′-hydroxyphenyl) benzoxazole and 2-(2′-hydroxyphenyl) benzothiazole. Bull Kor Chem Soc 2009;30:2865–6.
[13] Sonia RV, Crr M, Manuel M, Flor RP. Excited-state intramolecular proton transfer in 2-(3′-Hydroxy-2′-pyridyl)benzoxazole. Evidence of coupled proton and charge transfer in the excited state of some o-hydroxyarylbenzazoles. J Phys Chem A 2007;111:1814–26.
[14] Toshiyuki I, Atsuya M, Yoshihiro S, Tomoo S, Yoshinobu N, Tatsuo A. Excited-state intramolecular proton transfer of naphthalene-fused 2-(2′-hydroxyaryl) benzazole family. J Phys Chem A 2010;114:1603–9.
[15] Ajaykumar K, Sangamesh AP, Prema SB. Synthesis, characterization, DNA cleavage and in vitro antimicrobial studies of La(III), Th(IV) and VO(IV) complexes with Schiff bases of coumarin derivatives. Eur J Med Chem 2009;44:2904–12.

[16] Frisch MJ, Trucks GW, Schlegel HB, Scuseria GE, Robb MA, Cheeseman JR, et al. Gaussian 09, revision D.01. Wallingford, CT: Gaussian Inc.; 2009.
[17] Sun WH, Li SY, Hu R, Qian Y, Wang SQ, Yang GQ. Understanding solvent effects on luminescent properties of a triple fluorescent ESIPT compound and application for white light emission. J Phys Chem A 2009;113:5888–95.
[18] Signore G, Nifosi R, Albertazzi L, Storti B, Bizzarri R. Polarity-sensitive coumarins tailored to live cell imaging. J Am Chem Soc 2010;132:1276–88.
[19] Huang ST, Jian JL, Peng HZ, Wang KL, Lin CM, Huang CH, et al. The synthesis and optical characterization of novel iminocoumarin derivatives. Dyes Pigments 2010;86:6–14.
[20] Han F, Chi LN, Wu WT, Liang XF, Fu MY, Zhao JZ. J Photoch Photobiol A 2008;196:10–23.
[21] Park SY, Ebihara M, Kubota Y, Funabiki K, Matsui M. Dyes Pigments 2009;82:258–67.
[22] Kowalczyk T, Lin ZL, Voorhis TV. J Phys Chem A 2010;114:10427–34.
[23] Zhao GJ, Liu JY, Zhou LC, Han KL. Site-selective photoinduced electron transfer from alcoholic solvents to the chromophore facilitated by hydrogen bonding: a new fluorescence quenching mechanism. J Phys Chem B 2007;111:8940–5.
[24] Han F, Chi L, Liang X, Ji S, Liu S, Zhou F. 3,6-Disubstituted carbazole-based bisboronic acids with unusual fluorescence transduction as enantioselective fluorescent chemosensors for tartaric acid. J Org Chem 2009;74:1333–6.
[25] Ji S, Yang J, Yang Q, Liu S, Chen M, Zhao J. Tuning the intramolecular charge transfer of alkynylpyrenes: effect on photophysical properties and its application in design of OFF–ON fluorescent thiol probes. J Org Chem 2009;74:4855–65.
[26] Zhang X, Chi LN, Ji SM, Wu YB, Song P, Han KL, et al. Rational design of d-PeT phenylethynylated-carbazole monoboronic acid fluorescent sensors for the selective detection of α-hydroxyl carboxylic acids and monosaccharides. J Am Chem Soc 2009;131:17452–63.
[27] (a) Shao J, Guo H, Ji S, Zhao J. Styryl-BODIPY based red-emitting fluorescent OFF-ON molecular probe for specific detection of cysteine. Biosens Bioelectron 2011;26:3012–7;
(b) Guo H, Jing Y, Yuan XL, Jia SM, Zhao JZ, Li XH. Highly selective fluorescent OFF–ON thiol probes based on dyads of BODIPY and potent intramolecular electron sink 2,4-dinitrobenzenesulfonyl subunits. Org Biomol Chem 2011;9:3844–53.
[28] (a) Ji S, Wu W, Wu W, Song P, Han K, Wang Z, et al. Tuning the luminescence lifetimes of ruthenium(II) polypyridine complexes and its application in luminescent oxygen sensing. J Mater Chem 2010;20:1953–63;
(b) Wu W, Wu W, Ji S, Guo H, Wang X, Zhao J. The synthesis of 5,10,15,20-tetraarylporphyrins and their platinum(II) complexes as luminescent oxygen sensing materials. Dyes Pigments 2011;89:199–211;
(c) Ji S, Guo H, Yuan X, Li X, Ding H, Gao P, et al. A highly selective OFF-ON red-emitting phosphorescent thiol probe with large Stokes shift and long luminescent lifetime. Org Lett 2010;12:2876–9;
(d) Wu W, Wu W, Ji S, Guo H, Zhao J. Observation of room-temperature deep-red/near-IR phosphorescence of pyrene with cycloplatinated complexes: an experimental and theoretical study. Eur J Inorg Chem; 2010:4470–82;
(e) Wu W, Cheng C, Wu W, Guo H, Ji S, Song P, et al. Tuning the emission colour of triphenylamine-capped cyclometallated platinum(ii) complexes and their application in luminescent oxygen sensing and organic light-emitting diodes. Eur J Inorg Chem; 2010:4683–96;
(f) Wu W, Wu W, Ji S, Guo H, Song P, Han K, et al. Tuning the emission properties of cyclometalated platinum(II) complexes by intramolecular electron-sink/arylethynylated ligands and its application for enhanced luminescent oxygen sensing. J Mater Chem 2010;20:9775–86;
(g) Sun H, Guo H, Wu W, Liu X, Zhao J. Coumarin phosphorescence observed with *N^ N* Pt(II) bisacetylide complex and its applications for luminescent oxygen sensing and triplet–triplet-annihilation based upconversion. Dalton Trans 2011;40:7834–41;
(h) Sun J, Wu W, Guo H, Zhao J. Visible-light harvesting with cyclometalated iridium(iii) complexes having long-lived ^{3}il excited states and their application in triplet–triplet-annihilation based upconversion. Eur J Inorg Chem; 2011:3165–73.
[29] Iijima T, Momotake A, Shinohara Y, Sato T, Nishimura Y, Arai T. Excited-state intramolecular proton transfer of naphthalene-fused 2-(2′-hydroxyaryl)benzazole family. J Phys Chem A 2010;114:1603–9.
[30] Ikegami M, Arai T. Photoinduced intramolecular hydrogen atom transfer in 2-(hydroxyphenyl)benzoxazole and 2-(2-hydroxyphenyl)benzothiazole studied by laser flash photolysis. J Chem Soc Perkin Trans 2002;2:1296–301.
[31] Zhao GJ, Chen RK, Sun MT, Liu JY, Li GY, Gao YL, et al. Photoinduced intramolecular charge transfer and S2 fluorescence in thiophene-π-conjugated donor–acceptor systems: experimental and TDDFT studies. Chem Eur J 2008;14:6935–47.